ELSEVIER

International Journal of Refrigeration 27 (2004) 248–254

REVUE INTERNATIONALE DU FROID
INTERNATIONAL JOURNAL OF
refrigeration

www.elsevier.com/locate/ijrefrig

Particle deposition near ceiling induction outlets

H. Timmer, M. Zeller*

Institute of Heat Transfer and Air Conditioning, RWTH Aachen University, Eilfschornsteinstrasse 18, 52056 Aachen, Germany

Received 7 May 2003; received in revised form 9 October 2003; accepted 15 October 2003

Abstract

Particle deposition on ceilings close by ventilation outlets is a well-known and bothersome problem in the ventilation industry. This paper reveals the mechanisms causing the soiling of induction outlets and offers countermeasures. Experimentally verified CFD-calculations are performed to gain insight into the processes leading to particle deposition. It shows that the room air that is being induced by the entering airflow transports particles from the room to the ceiling where they deposit due to turbulent interaction forces. Other forces such as electro- and thermophoresis are negligible. An experimental technique is proposed to visualize the soiling patterns of an outlet by photographing deposited sodium chloride crystals. These tracer-particles stem from an atomizer and aerodynamically behave like the particles responsible for the soiling of ceilings in reality. Using image processing, suitable statistics describing the tendency of an outlet to attract particles can be derived from the pictures.

Keywords: Air conditioning; Air diffuser; Induction; Contamination; Particle; Process; Measurement

Dépôts de particules près des bouches de soufflage des diffuseurs d'air à induction en plafond

Mots clés : Conditionnement d'air ; Diffuseur d'air ; Induction ; Contamination ; Particule ; Procédé ; Mesure

1. Introduction

Ceiling induction outlets are a popular element in building to provide a room with fresh air. In the flow direction behind the outlet, dirt particles deposit on the ceiling and form characteristic textures that are optically displeasing and create considerable renovation costs (Fig. 1). Moreover, the occupants get the impression that the fresh air from the HVAC-system is polluted although this is not the case.

2. Characterization of dust depositions

Investigations in literature agree that the particles stem from the room itself [1–3]. Most particles found in indoor air are significantly smaller than 5 μm. However, scanning electron microscopy reveals that the particles responsible for the visible soiling are disc-shaped with a projected diameter of more than 20 μm (Fig. 2). They behave aerodynamically like water spheres with an aerodynamic diameter of about 5–15 μm. Most particles presumably are of organic origin

* Corresponding author. Member of IIR Commission E1. www.wuek.rwth-aachen.de Tel.: +49-241-80-95400; fax: +49-241-80-92143.

E-mail address: zeller@wuek.rwth-aachen.de (H. Timmer).

0140-7007/$35.00
doi:10.1016/j.ijrefrig.2003.10.003

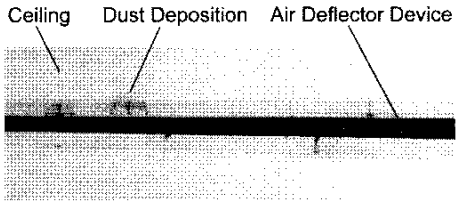

Fig. 1. Soiled ceiling induction outlet, upward view against the ceiling.

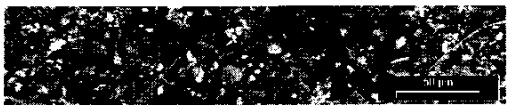

Fig. 2. Microscopy of deposited particles.

since they contain a high proportion of carbon and oxygen [2].

3. Methodology

The mechanisms causing particle deposition can be modelled both experimentally with a monodisperse fluorescent aerosol and numerically by computational fluid dynamics (CFD). All examinations are performed in a test chamber with a floor space of 4×6 m^2 and a height of 2.8 m. It is equipped with the ceiling induction outlet in Figs. 3 and 4 consisting of an extruded aluminium profile with plastic cylinders of 15 cm length comprised of apertures that are separated by webs. Along the apertures air enters the room at an acute angle against the ceiling that can be adjusted by turning the plastic cylinders around their symmetry axis. In

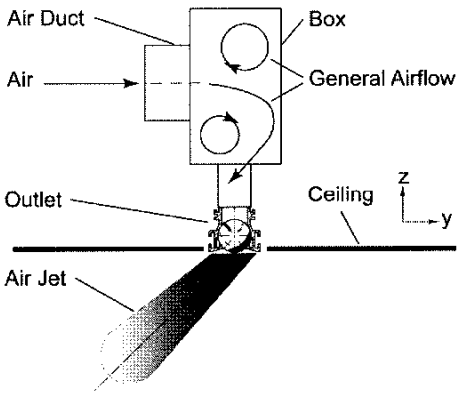

Fig. 3. Functional principle of the investigated outlet.

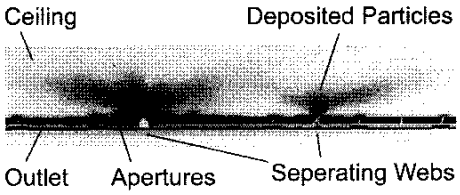

Fig. 4. Experimental soiling pattern.

the investigations presented below, all elements are equally adjusted so that they are blowing the air in the same direction at an inlet angle of approximately 45° and a volume flow of 100 m^3/mh. A recirculation emerges between the air jet and the ceiling before the jet attaches to the ceiling after a few centimetres because of the Coanda effect.

4. Experiment

The processes can be modelled with a monodisperse, crystalline, fluorescent aerosol generated in an ultrasonic atomizer. This technique is much more efficient than classic analyses with spray guns because it delivers quantitative deposition data and reduces the contamination of the test chamber. The particle mass deposited on the ceiling can be measured with a spectrofluorometer down to 100 pg [2]. These quantitative measurements allow a validation of the numerical simulation.

Since the deposited crystals reflect incident light, it is possible to photograph the soiling textures on the surface by using a flashlight for illumination. Thus a quick impression of the optical effect and the mass distribution can be obtained as the inverted photograph in Fig. 4 shows. Areas with a higher mass load appear darker in the picture.

It becomes clear from the picture that particles deposit mostly behind the webs. Laser-Doppler-Anemometry (LDA) shows that the turbulent kinetic energy reaches its maximums underneath these areas. A fluorescence analysis delivers the fraction of deposited particles (Fig. 5), i.e. the particle mass found on the surface divided by the surface area and the total particle mass injected into the test chamber.

Up to a certain degree, larger particles are likelier to deposit due to the higher drag force. When the diameter and thus the particle mass increase further, gravity prevails and leads to a decrease in deposition rates. This is why 9 μm particles have a higher deposition probability than 5 μm and 12 μm particles.

Further parameter variations yield a decrease of dirt deposition at steeper inlet angles against the ceiling and an increase with inlet velocity or volume flow.

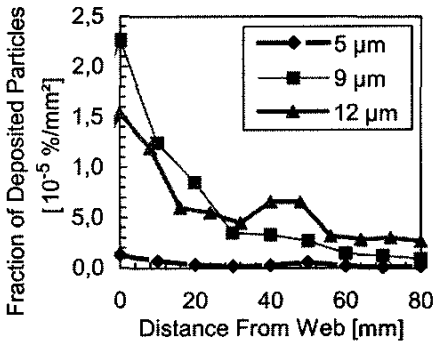

Fig. 5. Experimental deposition probability for three particle sizes.

5. Numerical simulation

Comparisons of CFD-calculations with LDA-measurements show that the use of a non-isotropic turbulence model and a sufficiently fine grid resolution at the ceiling are crucial for a realistic representation of the flow. Therefore, the Reynolds-Stress-Model (RSM) and no wall functions are used for calculation. The airflow inside the ventilation outlet has to be taken into account because it strongly influences the flow adjacent to the outlet inside the room. That way the inlet boundary conditions are sufficiently far away from the flow region of interest. The calculations were performed with the CFD-Code FLUENT/V on a Linux Cluster containing 10 Pentium® Processors (266 MHz–1.4 GHz). Mesh sizes ranged from 300 000 to 1 million cells depending on the symmetry of the given geometry.

Fig. 6 shows the calculated properties of the flow in an upward view against the ceiling. On the right and left hand side one finds the velocity vectors in two symmetry planes in the middle of the aperture and in the middle of the web. The round surface underneath the aperture of the ceiling induction outlet is an iso-surface of constant turbulent kinetic energy that encloses the regions of high turbulence. Inside the surface, turbulence is stronger than outside. The air jet is attached to the wall after a short distance and induces room air at its borders. This causes an upward flow underneath the jet which reaches the ceiling behind the web. Due to the shear stress turbulence emerges under the web and at a larger distance from the ceiling below the main flow.

Particle deposition on the ceiling can be calculated with a Lagrangian tracking routine which also allows a scrutiny of individual particle tracks. Each particle that hits the ceiling is assumed to adhere. This is a realistic supposition for the particle sizes considered. Matida et al. [4] report the available turbulence models to over-predict particle deposition from turbulent flows at low Reynolds numbers. Although the RSM comes closer to reality than k, ϵ based models, the deposition rates are larger in the calculations (Fig. 7) than in the experiments (Fig. 5). However, the qualitative agreement is satisfactory.

It is feasible to improve the results marginally with a higher grid resolution below the ceiling, but this rapidly increases the computational effort. Another improvement concerns the RSM, which generally calculates the eddy lifetime from the arithmetic mean of the fluctuation velocities in the three room coordinates. However, deposition is caused only by the wall-normal velocity component which is the smallest due to damping effects. It is therefore more realistic to use the minimum fluctuation velocity component instead. In doing so, lower deposition rates will be achieved.

5.1. Large eddy simulation

Further improvements can only be achieved with Large Eddy Simulation (LES) which resolves not only the mean flow but also the turbulent eddies larger than a specified scale. A turbulence model is only applied to the smaller energy-dissipating eddies that do not affect the overall flow. As a consequence, transient calculations have to be performed and geometrical symmetry cannot be used to reduce the calculated area since the

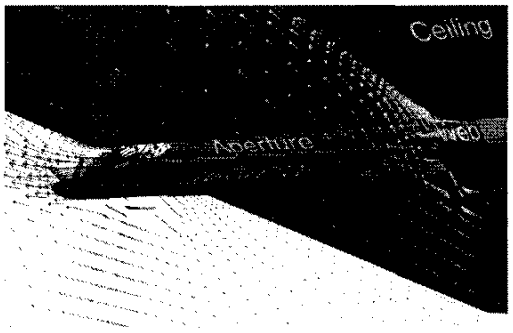

Fig. 6. CFD-calculations: airflow (vectors) and turbulence (surface underneath the aperture).

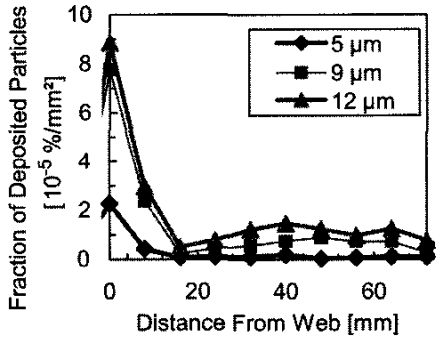

Fig. 7. Calculated deposition probability (Reynolds stress model).

turbulent structures are not symmetric in the planes of geometrical symmetry. This results in a larger calculation grid and tremendously increases the computational effort. For the given boundary conditions, LES calculations with a time step of 0.5–1 ms were performed. The calculations took several weeks although four processors of 1.4 GHz each were used simultaneously.

Each picture in Fig. 8 shows the y-velocities (direction of main flow) in three parallel geometrical symmetry planes in the middle of the outlet and the web for several time steps. The imaginary spectator of the scene sits on the roof of the test chamber and watches the flow in a downward view through a transparent ceiling. The ceiling induction outlet is located in the black region on top of each picture. In opposite to the RSM-calculations (Fig. 6), the flow field is clearly unsteady and the air jet does not stick so closely to the ceiling.

The trajectories of particles with a diameter of 9 μm were calculated simultaneously with the airflow. The deposition rates are much smaller (Fig. 9) than in the RSM calculations (Fig. 7) and agree better with the experiments (Fig. 5) in the area behind the web. Due to the larger distance between the air jet and the ceiling, no particles hit the ceiling behind the openings of the outlet. It can be assumed that particle deposition in this area is due to turbulence caused by a small misalignment between the ceiling and the induction outlet in the experiments.

5.2. Thermo- and electrophoresis

It is suspected in the literature that thermal [3] and electrical forces [5] augment the dirt deposition on building surfaces. The thermophoretic force acts on a particle suspended in a gas with a temperature gradient [6]. It is the driving force behind the sooting of an oil lamp: the carbon particles are dragged from the hot smoky flame towards the cold glass body. In an electric field, a charged particle is accelerated by electrophoretic forces. The Lagrangian particle tracking approach allows inclusion of both forces into the integration of the force balance of an individual particle.

Realistic boundary conditions for temperature and charge distributions at the ceiling are hard to find. Therefore, assumptions have to be made for evaluating the maximum influence both forces may have on dirt deposition. In the case of thermophoresis, the air jet and the ceiling are simulated to be 10 K cooler than the room air. In the case of electrophoresis, ceiling and particle carry a certain percentage between 0 and 10% of the maximum possible charge of ABS-plastics ($-1.65 \cdot 10^{-8}$ C/cm^2 [7]) or latex particle of 5 μm ($\pm 3.01 \cdot 10^{-17}$ C [8]) respectively.

In the calculations with the RSM, thermophoresis increases deposition by only 30% for a particle diameter of 1 μm. With augmenting diameter, the influence declines and vanishes for particles of 5 μm and larger that cause the visible soiling.

When it comes to electrophoresis one has to distinguish between attraction and repulsion. Fig. 10 shows the fraction of calculated particles depositing on the ceiling in case of repulsion (negative x-axis) and attraction (positive x-axis). If the ceiling and the particles are equally charged, i.e. both negative or positive, the electric force causes a repulsion which insignificantly compensates other forces acting towards the ceiling. In the opposite case of an electric attraction, which means that the ceiling and the particle carry opposite charges, electrophoresis acts stronger but nonetheless weaker than the other forces. At 10% of the maximum charge load deposition increases by only 30% for 5 μm particles (Fig. 10). Most of these additionally deposited particles hit the ceiling in regions where no contamination was found in the experiments which is an indication that the assumed charges are considerably larger than in reality. As in the case of thermophoresis, the influence even diminishes for larger particles.

6. Analysis

With the above findings, the soiling of induction outlets can be explained. Particles are whirled up from a surface and remain dispersed in the air until they settle again. However, a very few reach the inductive flow underneath the outlet and are transported upwards. Behind the webs, the particles follow the airflow to the turbulent eddies that lie right below the ceiling (Fig. 6). Those eddies accelerate the particles towards the ceiling and cause deposition. At a certain distance from the webs, the turbulent eddies on the lower side of the air jet only suffice to thrust a particle into the vortex between the air jet and the ceiling (Fig. 6). From here, some particles may then be accelerated towards the ceiling.

7. Countermeasures

As we have seen, turbulence is the driving force behind the soiling of ceilings; other forces such as thermo- and electrophoresis are negligible. However, neither turbulence nor the induction of particles with the induced room air can be prevented since both mechanisms are deliberate characteristics of mixed ventilation. A solution to the problem must be sought individually during the construction of an outlet by ensuring that the zones of high turbulence are positioned at an adequate distance from the ceiling and the induction of room air.

The tools presented so far do not facilitate the development of a clean outlet. Both the experimental

technique and the CFD-calculations are too sumptuous since they take too much time and effort to pursue.

8. New experimental approach

Instead of using costly and time-consuming fluorescence photometry, it is possible to determine the mass load from the photograph of the deposited test particles (Fig. 4) [9]. The picture is taken with a digital camera and illuminated with the integrated flashlight. Several influences on the photograph have to be corrected afterwards with an image processing software in order to gain an image matrix containing grey levels that are a linear function of the mass load at the corresponding point. First, the gamma correction imposed by the

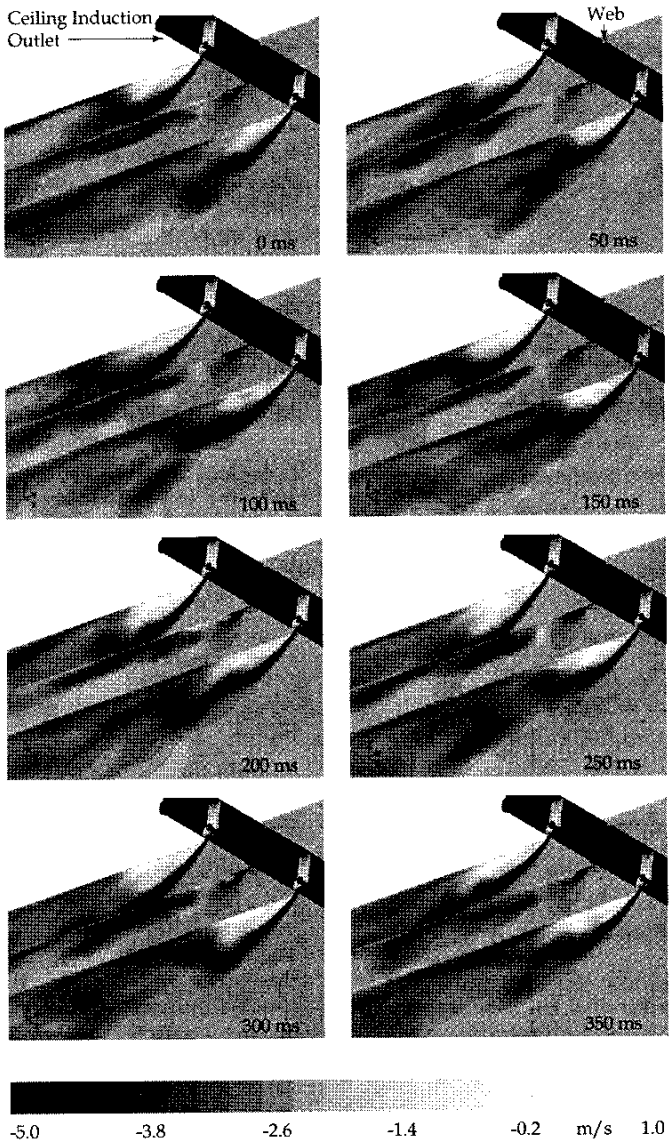

Fig. 8. Calculated y-velocities (direction of the main flow) for various time steps in three planes of geometrical symmetry (large eddy simulation).

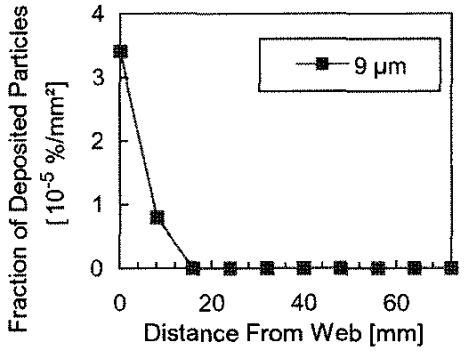

Fig. 9. Calculated deposition probability (large eddy simulation).

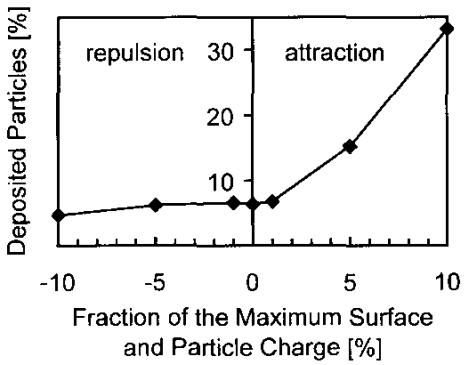

Fig. 10. Electrophoresis, 5 µm particles.

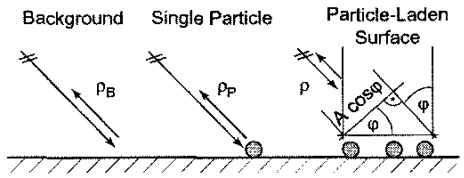

Fig. 11. Reflection model.

camera is removed so that the grey levels in the corrected digital image are proportional to the luminous intensity.

The photograph cannot be taken perpendicularly to the ceiling since the background reflection would outweigh the reflection from the particles. Photographing under an acute angle however delivers a perspective projection of the surface. In order to assign correct surfaces to the intensities of the pixels, a geometrical correction has to be performed. Therefore, the image transformation matrix is calculated from a least squares problem correlating several corresponding points in the picture of the soiled surface and another picture taken perpendicularly to the ceiling. With the known transformation matrix, the photograph of the soiled ceiling can be transformed. In the process of this correction, the angle of photography can also be computed.

In the time needed to create visible deposition the crystals do not overlap which is a premise for the further procedure. For a lower soiling of the test chamber, the crystalline aerosol can be generated with sodium-chloride instead of fluorescein since fluorescence is not needed here. The back-reflectivity ρ of a particle-laden surface A can be described as the combination of the reflectivity of the background ρ_B and a single particle ρ_P (Fig. 11).

Typically, the flashlight creates a non-uniform illumination of the scene. Thus the mass load must be derived from the quotient between the grey levels in the image matrix G and those of the clean background G_B which can be computed from G by cluster analysis [10]. The resulting measure is independent of the luminosity E.

$$\frac{G}{G_B} = \frac{\rho E}{\rho_B E} = \frac{\rho}{\rho_B}$$

The backscattered light is

$$\rho E A \cos\varphi = \rho_B E(A\cos\varphi - A_P) + \rho_P E A_P$$

It depends on the area covered by particles A_P, the total surface A and the incident angle φ. The mass load m'' (kg/m^2) is proportional to the quotient between A_P and A.

$$m'' = C_1 \frac{A_P}{A}$$

Consequently, the total reflectivity can be calculated from the mass load by introducing a new constant C_2

$$\rho = \rho_B + \frac{\rho_P - \rho_B}{C_1} \frac{m''}{\cos\varphi} = \rho_B + C_2 \frac{m''}{\cos\varphi}$$

and vice versa, the mass load can be derived from the matrices of the greyscale images

$$\frac{G}{G_B} = 1 + \frac{m''}{C \cdot \cos\varphi}$$

The constant C includes the reflection coefficients and the particle size. It takes values between 0.003 m^2/kg (NaCl, 9 µm) and 0.008 m^2/kg (fluorescein, 12 µm). The method is expected to be quite reliable when the results of at least four pictures taken from different angles are averaged. For those photographs a maximum ratio of variance to arithmetic mean of 42% was observed in the experiments. This ratio can be interpreted as the expected error when the mass load is calculated from a single photograph.

9. Characteristic value of soiling

The tendency of a linear induction outlet towards attracting particles can be defined as the deposited mass per inlet length L normalized with the total mass m_{tot} blown into the test chamber per total inlet length L_{tot}. This nondimensional quantity

$$\zeta_M = \frac{L_{tot}}{m_{tot}L}\int\int_A m''(x,y)\mathrm{d}x\mathrm{d}y$$

is therefore appointed "mean dirt load ratio".

The mass load does not sufficiently describe the visual impact of the deposition pattern on the observer because visual perception is essentially based on contrast. Therefore, an additional ratio based on the derivative of the mass load is proposed. A sobel filter f [11] is used to calculate the mean derivative from the mass load matrix. The "mean dirt contrast ratio"

$$\zeta_C = \frac{L_{tot}}{m_{tot}L}\int\int_A f[\nabla m''(x,y)]\mathrm{d}x\mathrm{d}y$$

is thus a measure for the visually perceived contrasts caused by the distribution of the deposited particles.

Some case studies to the method are presented in [9].

10. Example of a countermeasure

Drilling a hole into the plastic cylinders of the outlet on both sides of the webs (Fig. 12) has proven an effective countermeasure to reduce particle deposition behind the webs for the configuration at topic. A small fraction of the air stream passes through the drillings and destroys the upward airflow underneath the webs without changing the intended main flow inside the room. Thus less particles are transported to the turbulent eddies behind the webs. This simple remedy reduces the mean dirt load ratio from $\zeta_M = 0.43$ to 0.009% and the mean dirt contrast ratio from $\zeta_C = 19.28$ to 1.45/m. However, the effectiveness of this countermeasure is limited to the specific outlet geometry and does not present a universal solution.

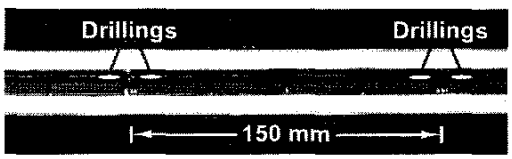

Fig. 12. Possible countermeasure.

11. Conclusion

The soiling of ceiling induction outlets is mainly caused by the features of mixed ventilation, i.e. turbulence and induction. A solution to the problem can only be found individually depending on the geometry of the particular outlet. The search for a clean outlet is facilitated by the proposed optical technique which is suitable for an efficient deposition assessment in the ventilation industry.

Acknowledgements

We are grateful that the main part of this work has been supported by the "Forschungsvereinigung für Luft- und Trocknungstechnik e.V. (FLT)" and the "Bundesminister für Wirtschaft" via "Arbeitsgemeinschaft Industrieller Forschungsvereinigungen (AiF)".

References

[1] Fichter, RH, Knorr, T, Roth, HW. Deckenverschmutzung durch Luftauslässe. CCI 1996;36–8.
[2] Timmer, H, Zeller, M, Jordan, F, Neumann, S, Fissan, H. Überprüfung der Verschmutzung im Nahbereich von Deckenluftdurchlässen. ki Luft- und Kältetechnik 2001;256–61.
[3] Finke, U, Fitzner, K. Beurteilung der Deckenverschmutzung durch Schlitzdurchlässe. DKV-Tagungsband 1996;119–28.
[4] Matida EA, Nishino K, Torii K. Statistical simulation of particle deposition on the wall from turbulent dispersed pipe flow. International Journal of Heat and Fluid Flow 2000:389–402.
[5] Vogel KH. Wie die Decke sauber bleibt. CCI 1995;9:27–9.
[6] Talbot L, Cheng RK, Schefer WR, Willis DR. Thermophoresis of particles in a heated boundary layer. Journal of Fluid Mechanics 1980:737–58.
[7] Bauser, H. Static Electrification of Organic Solids. In: Behrens D, Fischbeck K, editors. Frankfurt: DECHEMA-Monographien; 1974. p. 11–8.
[8] Muhr, W. Elektrostatische Aufladung verschiedener Teststäube. Chemie Ingenieur Technik 1976;581.
[9] Timmer, H. Deckenverschmutzung durch Luftdurchlässe. Dissertation RWTH Aachen University. Shaker Verlag; 2003.
[10] Müller, RK, Ettemeyer, A, Ott, R, Saackel, L, Stoehrel, HP. Digitale Bildverarbeitung in der experimentellen Spannungsanalyse und in der Produktionskontrolle. Kontakt & Studium; 1990.
[11] Müller, RK, Ettemeyer, A, Ott, R, Saackel, L, Stoehrel, HP (1990). Digitale Bildverarbeitung in der experimentellen Spannungsanalyse und in der Produktionskontrolle. In: Bartz WJ, editor. Ehningen (Germany): Kontakt & Studium; 1990. p. 42.